Available online at www.sciencedirect.com
SCIENCE DIRECT®
Ocean Modelling 6 (2004) 379–403
Ocean Modelling
www.elsevier.com/locate/omodol

# A generalized coordinate ocean model and a comparison of the bottom boundary layer dynamics in terrain-following and in *z*-level grids

Tal Ezer *, George L. Mellor

*Program in Atmospheric and Oceanic Sciences, Princeton University, P.O. Box CN710, Sayre Hall, Princeton, NJ 08544-0710, USA*

Received 14 November 2002; received in revised form 14 April 2003; accepted 14 April 2003

**Abstract**

Sensitivity studies with a new generalized coordinate ocean model are performed in order to compare the behavior of bottom boundary layers (BBLs) when terrain-following (sigma or combined sigma and *z*-level) or *z*-level vertical grids are used, but most other numerical aspects remain unchanged. The model uses a second-order turbulence closure scheme that provides surface and BBL mixing and results in a quite realistic climatology and deep water masses after 100 year simulations with a coarse resolution ($1^\circ \times 1^\circ$) basin-scale terrain-following grid. However, with the same turbulence scheme but using a *z*-level grid, the model was unable to produce dense water masses in the deep ocean. The latter is a known problem for coarse resolution *z*-level models, unless they include highly empirical BBL schemes.

A set of dense water overflow experiments with high-resolution grids (10 and 2.5 km) are used to investigate the influence of model parameters such as horizontal diffusivity, vertical mixing, horizontal resolution, and vertical resolution on the simulation of bottom layers for the different coordinate systems. Increasing horizontal diffusivity causes a thinner BBL and a bottom plume that extends further downslope in a sigma grid, but causes a thicker BBL and limited downslope plume extension in a *z*-level grid. A major difference in the behavior of the BBL in the two grids is due to the larger vertical mixing generated by the turbulence scheme over the step-like topography in the *z*-level grid, compared to a smaller vertical mixing and a more stably stratified BBL in the sigma grid. Therefore, the dense plume is able to maintain its water mass better and penetrates farther downslope in the sigma grid than in the *z*-level grid. Increasing horizontal and vertical resolution in the *z*-level grid converges the results toward those obtained by a much coarser resolution sigma coordinate grid, but some differences remain due to the basic differences in the mixing process in the BBL.


*Keywords:* Numerical modeling; Sigma coordinates; Ocean mixing

* Corresponding author. Tel.: +1-609-258-1318; fax: +1-609-258-2850.
*E-mail address:* ezer@splash.princeton.edu (T. Ezer).

1463-5003/$ - see front matter 
doi:10.1016/S1463-5003(03)00026-X

## 1. Introduction

Various types of ocean models with different vertical coordinate systems such as isopycnal, terrain-following (sigma) or $z$-level are being used for simulations of oceanic processes ranging from small-scale coastal dynamics to global climate change problems (e.g., see the recent reviews of developments in climate ocean models by Griffies et al. (2000); and developments in terrain-following ocean models by Ezer et al. (2002)). Moreover, model applications have expanded beyond their original intent; for example, sigma coordinate ocean models that traditionally were used in the past mostly for regional coastal simulations, are now being used for basin-scale and climate problems as well (Haidvogel et al., 2000; Hakkinen, 2000; Ezer and Mellor, 1997, 2000; Ezer, 1999, 2001). Therefore, an important question is: to what extent does the choice of the numerical model type affect simulation results? Several projects tried to answer this question by comparing the results of different models (usually operating by different groups at different institutions) under similar configurations and forcing. Such projects include for example, the Dynamics of North Atlantic Models (DYNAMO, Meincke et al., 2001), the Data Assimilation and Model Evaluation Experiments in the Gulf Stream region (DAMEE-GSR, Willems et al., 1994) and in the North Atlantic basin (DAMEE-NAB, Chassignet et al., 2000). A recent intercomparison initiative now underway is the Dynamics of Overflow Mixing and Entrainment project (DOME, see www.rsmas.miami.edu/personal/tamay/DOME/dome.html); the results presented here are part of this project. Aside from the difficulty of coordinating such multi-group intercomparison projects, there are inherent numerical differences between the models that make it very difficult to isolate the effect of vertical grid design. One solution is to perform a comparison of results obtained with generalized or hybrid models (Gerdes, 1993; Bleck, 2002; Mellor et al., 2002; Pietrzak et al., 2002; Rowley et al., 2002); this is the approach reported here using the generalized ocean model described by Mellor et al. (2002).

The DOME projet mentioned above was largely motivated by the increasing evidence that coarse resolution climate models (the majority of which historically used $z$-level grids) have difficulties in simulating deep water formation by density-driven down-slope overflow processes because of the step-like representation of topography (Gerdes, 1993; Beckmann and Döscher, 1997; Winton et al., 1998; Pacanowski and Gnanadesikan, 1998). This problem led to various attempts to either improve the representation of topography in $z$-level models by partial or shaved cells (Adcroft et al., 1997; Pacanowski and Gnanadesikan, 1998) or by adding artificial bottom boundary layers (BBLs) that allow overflows to "skip over" the steps of the $z$-level topography (Beckmann and Döscher, 1997; Campin and Goosse, 1999; Killworth and Edwards, 1999; Song and Chao, 2000). Terrain-following ocean models on the other hand, have a smooth representation of topography that allows a more natural treatment of BBL dynamics. Resolving the BBL in the ocean may be also important for the pressure compensation that drives the large-scale ocean circulation (Mellor and Wang, 1996). A recent study (Penduff et al., 2002) suggests, for example, that simply smoothing the topography in a $z$-level model results in more realistic simulations that closely resemble results obtained with a sigma-coordinate model. Therefore, sigma ocean models have been used, for example, for the simulations of the Mediterranean deep water formation (Zavatarelli and Mellor, 1995), the Mediterranean deep outflow into the Atlantic Ocean (Jungclaus and Mellor, 2000) and the Denmark Straites overflow (Jiang and Garwood,

1996; Jungclaus et al., 2001). Isopycnic coordinate ocean models can also be useful for simulations of density-driven overflows (e.g., Papadakis et al., 2003).

The main objectives of this study are: First, to test the generalized coordinate ocean model of Mellor et al. (2002) for various grids, resolutions and parameterizations, and second, to study the density-driven overflow process and the behavior of BBLs for different grids.

## 2. The generalized coordinate ocean model

The generalized ocean model used here is described in details by Mellor et al. (2002). This model is an extension of the free surface, three-dimensional, primitive equation numerical code of the Princeton Ocean Model (POM, Blumberg and Mellor, 1987). This version allows the replacement of the standard sigma coordinate system with a more general distribution of layers, $z = \eta(x, y, t) + s(x, y, k, t)$, where $z$ is the depth of layer $1 < k < kb$ at location $(x, y)$ and time $t$, $H$ is the water depth and $\eta$ is the free surface elevation. As special cases, a $z$-level system is $s = \sigma(k)[H_{\max} + \eta(x, y, t)]$, and a sigma coordinate system is $s = \sigma(k)[H(x, y) + \eta(x, y, t)]$, where $H_{\max}$ is the maximum depth and the relative distribution of vertical layers is $0 < \sigma(k) < -1$. A three-dimensional land/ocean mask replaces the two-dimensional mask of the sigma grid. Note that, the generalized terrain-following coordinates called $s$-coordinate system (Song and Haidvogel, 1994; Haidvogel et al., 2000) relays on analytical expressions for $s$ and is more general than the standard sigma grid, but it can not use stepped grids such as a $z$-level grid. Note also that the horizontal numerical grid is based on the staggered C-grid (Arakawa and Lamb, 1977), while $z$-level models often use the B-grid (Griffies et al., 2000).

Since the model subroutine that represents a user's defined function, $s$, is updated every time step, in principle, a time-varying adjustable grid that imitates isopycnal coordinates is possible, an option that has not yet been completed. Another potential grid may be a "stepped sigma" that replaces steep slopes in the sigma grid with vertical walls. This latter option may reduce pressure gradient errors over steep topography (Haney, 1991; Beckmann and Haidvogel, 1993; Mellor et al., 1994, 1998). Note however, that recent improvements in pressure gradient schemes can reduce these errors considerably (Chu and Fan, 1997; Ezer et al., 2002; Shchepetkin and McWilliams, 2003).

Mellor et al. (2002) tested models using an idealized basin with a shelf in the north and forcing that includes a steady, zonally averaged wind stress; the model was executed for 1 year period using three different grids, a $z$-level grid, a sigma grid, and a "$z$-plus-sigma" grid (Figs. 1 and 2). The latter grid has $z$-levels in the deep ocean that converge to form a fine grid near the sloping bottom, for better resolution of BBLs. As a first test of the model, we use exactly the same domain and grids as in Mellor et al. (2002), but add zonally averaged and meridionally varying surface heat flux and integrate the model for much longer period of 100 years. The model resolution is $1° \times 1°$, with 21 vertical layers. The aim is to see how the mean ocean thermal structure, including the mixed layer and deep water masses, are formed when using different grids. The initial temperature (in °C) depends only on $z$ and is defined by $T(x, y, z) = 5 + 15\exp(z/1000\text{ m})$. Salinity is constant at 35 psu. The zonal wind stress is defined by $\tau_x = -2 \times 10^{-4}\ \text{m}^2\,\text{s}^{-2} \sin(2\pi\Phi/60)$, where $\Phi$ is latitude. Surface heat flux forcing in the model includes both short wave radiation penetration

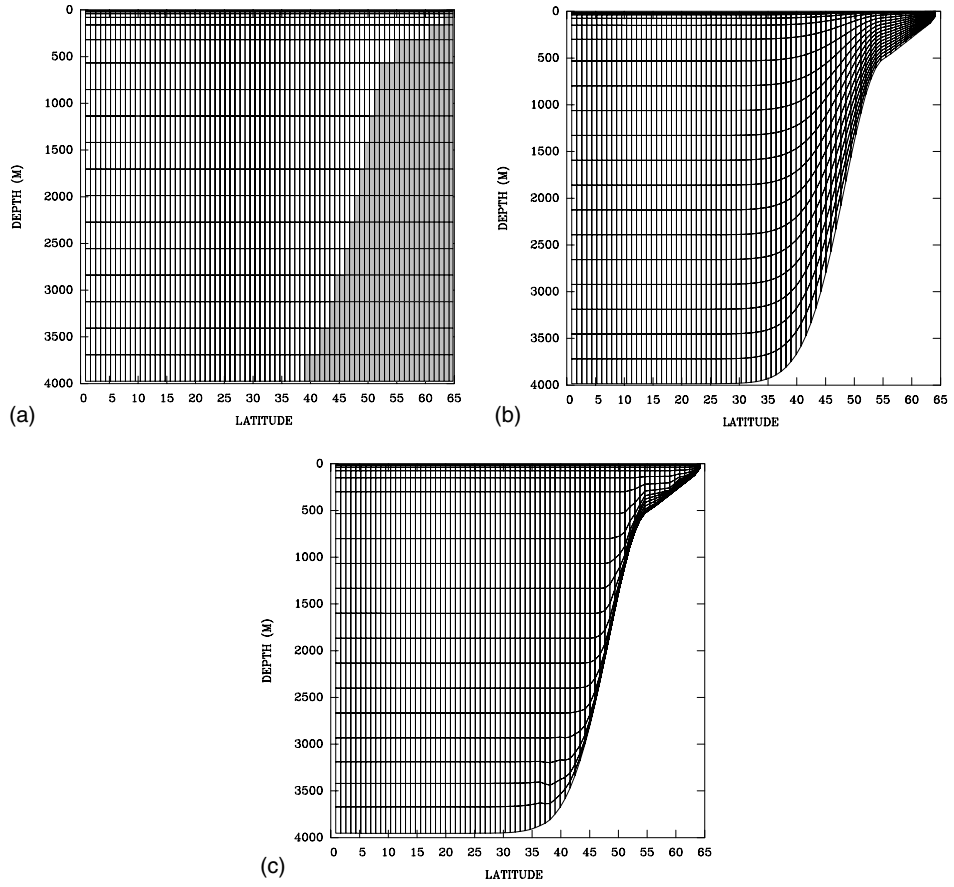


Fig. 1. Vertical grids used by the basin-scale generalized coordinate model of Mellor et al. (2002): (a) standard $z$-level grid, (b) standard sigma coordinate grid, (c) generalized $z$ plus sigma grid with enhanced BBLs.

and air–sea heat exchange that resemble the zonally averaged observed climatology; the applied net heat flux is a liner function of latitude, with 21 w m$^2$ (heating) at $\Phi = 0$ and $-27$ w m$^2$ (cooling) at $\Phi = 65°$N. Ezer (2000), Rochford et al. (2001) and others show the importance of including short wave radiation penetration in order to achieve realistic surface mixed layers in models that use the Mellor–Yamada (Mellor and Yamada, 1982) turbulence scheme.

Horizontal viscosity and diffusivity in the $z$-level grid are $(A_M, A_H) = (10^4, 0.2 \times 10^4)$ m$^2$ s$^{-1}$, typical values for $z$-level models of such resolution; this $z$-level model becomes unstable if smaller diffusivity is used (Mellor et al., 2002) or if the velocity-dependent Smagorinsky scheme (Smagorinsky, 1963) is used. Terrain-following models (Fig. 1b and c) on the other hand work best with as little along-sigma horizontal diffusion as possible in order to minimize unwanted diapycnal mixing so they use the Smagorinsky scheme with a Smagorinsky coefficient of 0.5 and $A_M/A_H = 0.2$. The diffusion is applied only to anomalies relative to the initial climatology in order to further reduce any along-slope diffusion (see Mellor and Blumberg (1985), Ezer and Mellor (2000) and Ezer (2001) for more information on the sensitivity of sigma models to diffusivity schemes). While the diffusion is not exactly the same for all grids, we prefer here to use the scheme

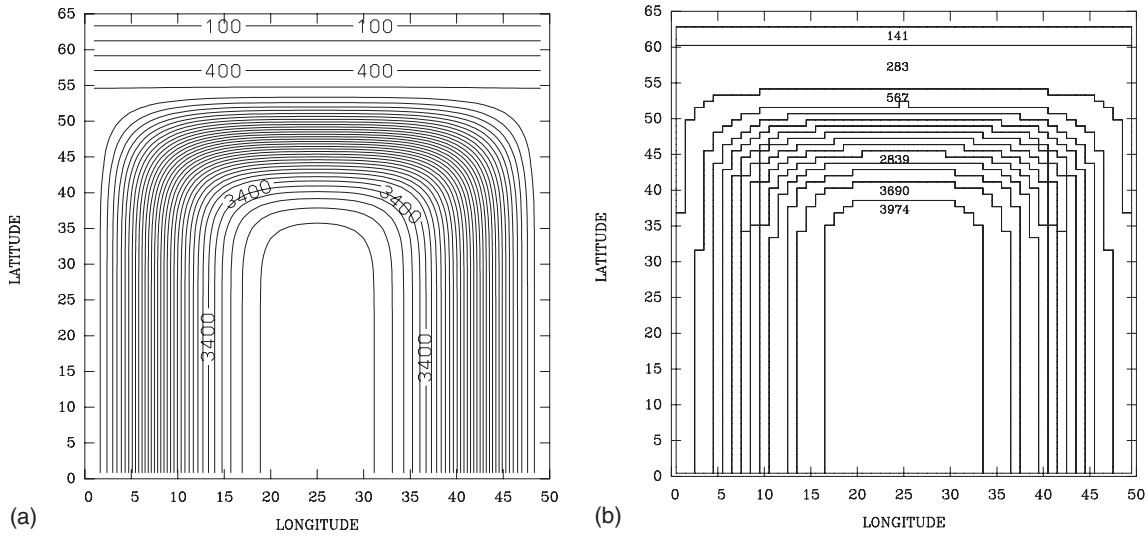


Fig. 2. Bottom topography (depth in meters) in the basin-scale domain as seen by (a) the sigma or the sigma plus $z$-level grids, and (b) the $z$-level grid.

that works best for each numerical model following the experience of Mellor et al. (2002). The smaller domain and shorter run time in the high-resolution experiments described later will allow us to use identical diffusivity values independent of the grid. The vertical mixing is based on the Mellor–Yamada turbulence scheme (Mellor and Yamada, 1982) for all grids, so there is no need to add a convective adjustment scheme, as often done in $z$-level models.

The final model temperatures in the three simulations after 100 years are shown in Fig. 3 together with the observed climatology (Levitus and Boyer, 1994). The structure of the mixed layer, which is shallower in the tropics and deeper in mid-latitudes, is quite realistic and similar in all cases. In mid and high latitudes the isotherms are vertical in the $z$-level (Fig. 3b), but tilted in the other grids (Fig. 3c and d) as in the observed climatology (Fig. 3a). The reason for this difference is that the cold water formed on the shelf tends to flow down-slope in the sigma and $z$-plus-sigma grids, but advects horizontally in the $z$-level model, creating hydrostatic instability and strong turbulent vertical mixing in the middle latitudes of the $z$-level model.

The temperatures in the deep ocean are apparently influenced strongly by the grid. The initial bottom temperature in the deep ocean was 5.3 °C. After 100 years integration the bottom temperature has increased slightly to 5.5 °C in the $z$-level model, but cooled to 3.2 °C in the sigma model, and to 4.2 °C in the $z$-plus-sigma model. Observations show temperatures around 3 °C between 2000 and 4000 m depth. In the $z$-level model, a thick intermediate water mass is formed between 1500 and 3000 m depths, but the cold shelf water did not reach the deeper near-bottom layers. In the two terrain-following grids (Fig. 3c and d) the cold shelf water from high latitudes penetrated downslope to form a cold bottom water mass similar to that observed. An interesting result is that the grid with better resolved BBLs (Fig. 3d) produced slightly less cold bottom water mass than the standard sigma grid did. This is due to the fact that the relatively coarse vertical

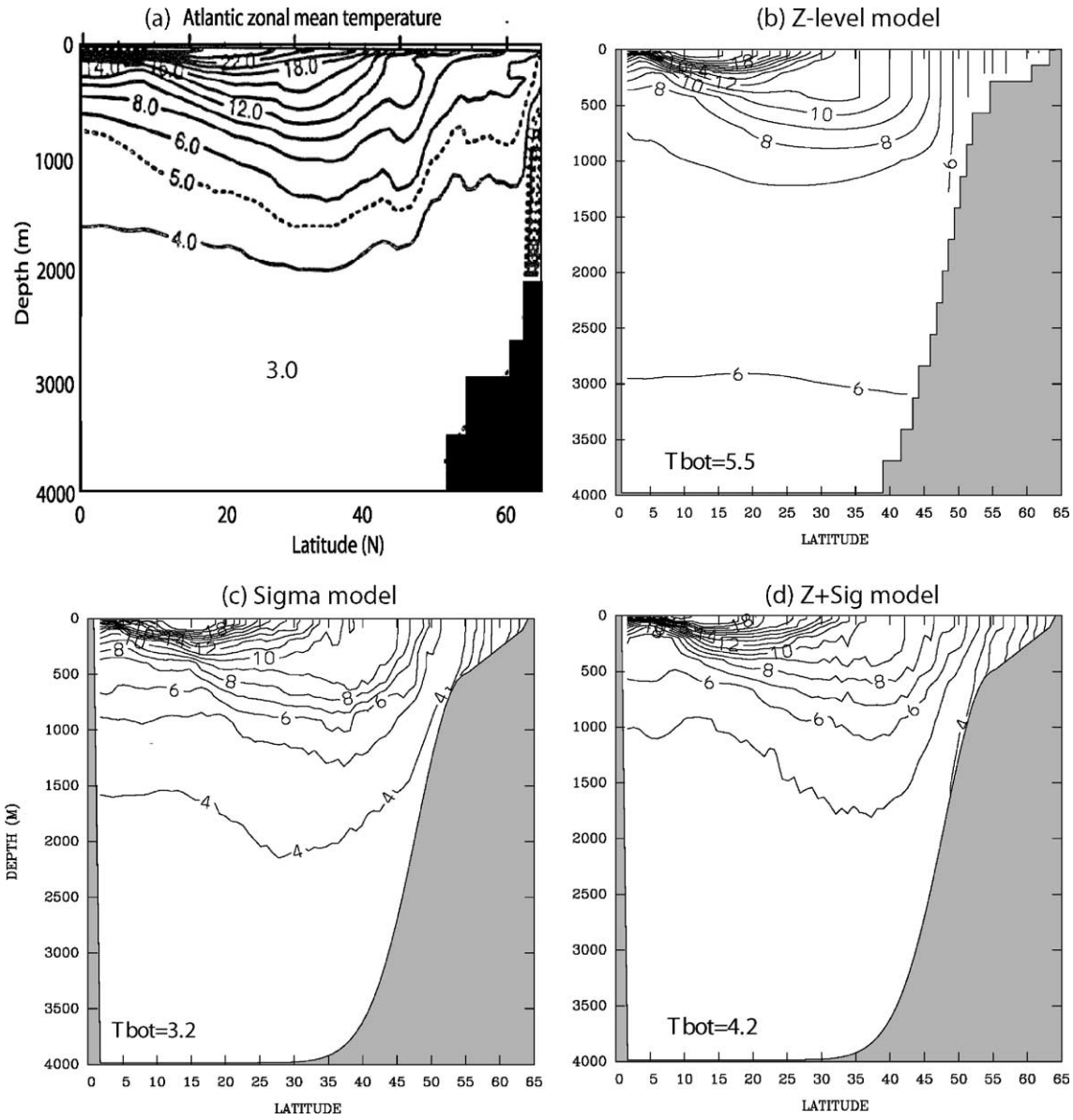


Fig. 3. (a) Observed zonal and annual mean temperature across the Atlantic Ocean (Levitus and Boyer, 1994). Model cross-section of temperature at the center of the domain (25° longitude) after 100 years simulations starting with no horizontal temperature gradients and using (b) *z*-level grid, (c) sigma coordinate grid, and (d) *z* plus sigma grid. Contour interval is 1 °C; final bottom temperature is indicated by "Tbot".

resolution in the sigma grid results in a thicker BBL and thus larger downslope transport of dense waters than that of the better resolved *z*-plus-sigma grid.

The experiments in this example agree with previous studies that show the difficulty of simulating density-driven down-slope flows with coarse resolution *z*-level models. The direct com-

parison with terrain-following ocean models using otherwise the same numerical schemes, shows considerable differences. Therefore, the downslope flow and mixing processes are further investigated in more details with higher resolution grids in order to better understand those differences. One expects that with finer grids the differences between simulations using different coordinate systems will be smaller, but this assumption needs to be tested.

## 3. High-resolution dense overflow simulations

### 3.1. The DOME configuration setup

These simulations are based on the standard configuration and setup for the intercomparison DOME project (see details of setup in the DOME web page mentioned in Section 1) using two different coordinate systems, a sigma grid and a $z$-level grid. The domain includes an idealized deep basin of $1100 \times 800$ km, maximum depth of 3600 m (except for the Z4 case, see Table 1), and a 1% steep slope which connects to a 100 km wide and 600 m deep embayment (Fig. 4a). While the experimental design aims to imitate deep water formation processes from say the Denmark Strait (Jungclaus et al., 2001; Girton and Sanford, in press), the configuration is quite idealized, so that direct model-data comparisons are not possible. Nevertheless, some of the basic characteristics of the model overflow, such as the maximum velocity, plume thickness and rate of descent are quite similar to the observed features, as will be shown later. The initial conditions include a background linear stratification and a dense water mass in the lower portion of the embayment (Fig. 4b). A linear equation of state (with constant salinity) is used so that the maximum density difference between the surface and the deepest layers, and between the surface and the dense bottom layer in the embayment are both $\Delta\rho = 2\ \mathrm{kg\,m^{-3}}$. The initial thickness of the dense water in the embayment is specified such that it is close to a geostrophical balance with a maximum of 300 m near the western wall of the embayment and exponentially decaying to zero near the eastern wall. Buffer zones with temperature relaxation are applied in the northern half of the embayment and

Table 1
Experiments done with the configuration of Fig. 4a

| Experiment (S, sigma grid; Z, $z$-level grid) | Horizontal resolution (km) | Number of layers (vertical resolution) | Diffusion coefficient ($A_H$, $m^2\,s^{-1}$) | Area of bottom plume (100 km)$^2$ | Average thickness of plume (m) |
|---|---|---|---|---|---|
| S1 | 10 | 50 (12–72 m) | $10^1$ | 13.4 | 304 |
| S2 | 10 | 50 (12–72 m) | $10^2$ | 13.3 | 244 |
| S3 | 10 | 50 (12–72 m) | $10^3$ | 14.6 | 276 |
| Z1 | 10 | 50 (50–100 m) | $10^1$ | 6.5 | 413 |
| Z2 | 10 | 50 (50–100 m) | $10^2$ | 7.5 | 414 |
| Z3 | 10 | 50 (50–100 m) | $10^3$ | 6.0 | 498 |
| S4 | 10 | 10 (60–360 m) | $10^2$ | 10.3 | 276 |
| Z4 | 2.5 | 88 (25 m) | $10^1$ | 9.0 | 272 |

The domain size is 1100 km × 800 km and maximum depth is 3600 m, except experiment Z4, which has a domain size of 1100 km × 400 km and maximum depth of 2200 m. The viscosity in all experiments is $A_M = 5A_H$. The bottom plume is defined by tracer concentration of 0.1 and larger.

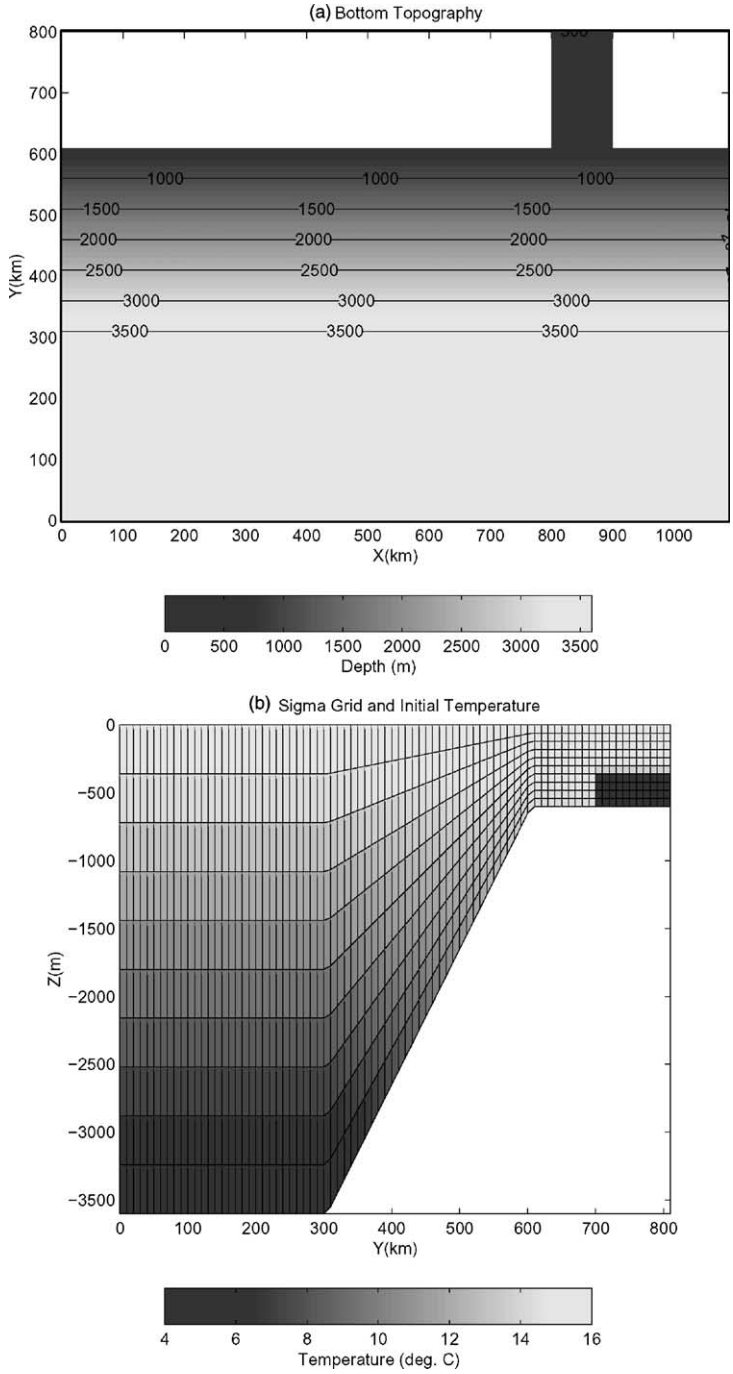


Fig. 4. (a) Top view of the bottom topography in the DOME experiments, and (b) a cross-sections of the initial temperature at $x = 800$ km and the distribution of vertical layers in the sigma coordinate (experiment S4).

near the east and west open boundaries. Boundary conditions for velocities include radiation conditions in the east and west open boundaries and an imposed southward velocity in the northern embayment so that the total southward transport of dense water from the embayment is 5 Sv (1 Sverdrup $= 10^6$ m$^3$ s$^{-1}$) for all experiments. The above conditions were developed jointly by the participants of the DOME project in order to minimize recirculation and mixing in the embayment itself and to allow a similar configuration to be implemented by different models.

For the sigma grid cases, S1–S3, and the $z$-level cases, Z1–Z3, the horizontal resolution of the grid is 10 km, and the number of vertical layers is 50 (Table 1). The sigma layers are evenly distributed (though in practical applications increase resolution near the bottom may be beneficial for this case). In the above $z$-level cases the vertical resolution in the region relevant to the location of the plume, between 200 and 1600 m depth, is 50 m; elsewhere, near the surface and in the very deep ocean (far from the plume) the resolution is 100 m (the minimum resolution required to resolve the slope). Two cases, S4 and Z4, are somewhat special and will be discussed later.

### 3.2. The effect of horizontal diffusivity

Mellor et al. (2002) showed that, because of the step-like topography, coarse resolution $z$-level models need larger horizontal diffusivity than do terrain-following models with smooth bottom, in order to maintain numerical stability. The high-resolution grid here allows us to reduce the horizontal diffusivity in the $z$-level model, and to test its effects on the simulations. Therefore, six experiments were conducted here, three for each coordinate system, using constant diffusivities of $A_H = 10^1$, $10^2$ and $10^3$ m$^2$ s$^{-1}$ (viscosity is $A_M = 5A_H$ in all cases). A Multidimensional Positive Definition Advection Transport Algorithm with reduced diffusivity (MPDATA, Smolarkiewicz, 1984) advection scheme is used. The diffusivity specified by $A_H$ is in addition to the small diffusivity inherited in the MPDATA scheme. The sigma grid remains relatively stable, with no additional diffusivity, but the $z$-level grid does need additional diffusivity to remain stable at that resolution. To help analyze the development of the dense water plume, a tracer, with value $c = 1$, was injected into the dense water in the embayment; initially $c = 0$ everywhere else.

The westward and down-slope propagation of the dense bottom plume in the sigma coordinate model involved not only bottom Ekman flows, but also the mixing due to eddies (Figs. 5 and 6), as previously indicated in the study of Jiang and Garwood (1996), using POM in a similar configuration. The Rossby radius of deformation here is about 45 km, so that eddies are marginally resolved with a 10 km grid. There are almost no eddies in the case with larger diffusivity of $A_H = 10^3$ m$^2$ s$^{-1}$, and the diffused front in this case causes a slower propagation of the plume (Fig. 7). When comparing the bottom plume in the sigma model to the $z$-level model after 40 days (only case Z2 is shown in Fig. 8, the other cases, Z1 and Z3, look very similar), the results are very different. In the $z$-level model the bottom plume is diffused and remains near the coast; eddies are weaker since the front of the plume is not sharp enough to support frontal instabilities.

Fig. 9 compares the cross section of the plume in the six experiments after 40 days. The sigma grid calculations (left panels) show much thinner plumes that extend further downslope than those of the $z$-level grid calculations (right panels). Increasing the horizontal diffusivities (from top to bottom in Fig. 9) causes thinner plumes in the sigma grids, but causes thicker plumes in the $z$-level grid, in particular near the downslope edge. The average thickness of the plume over the entire domain is about 250–300 m in the sigma grid calculations, but about 400–500 m in the $z$-level

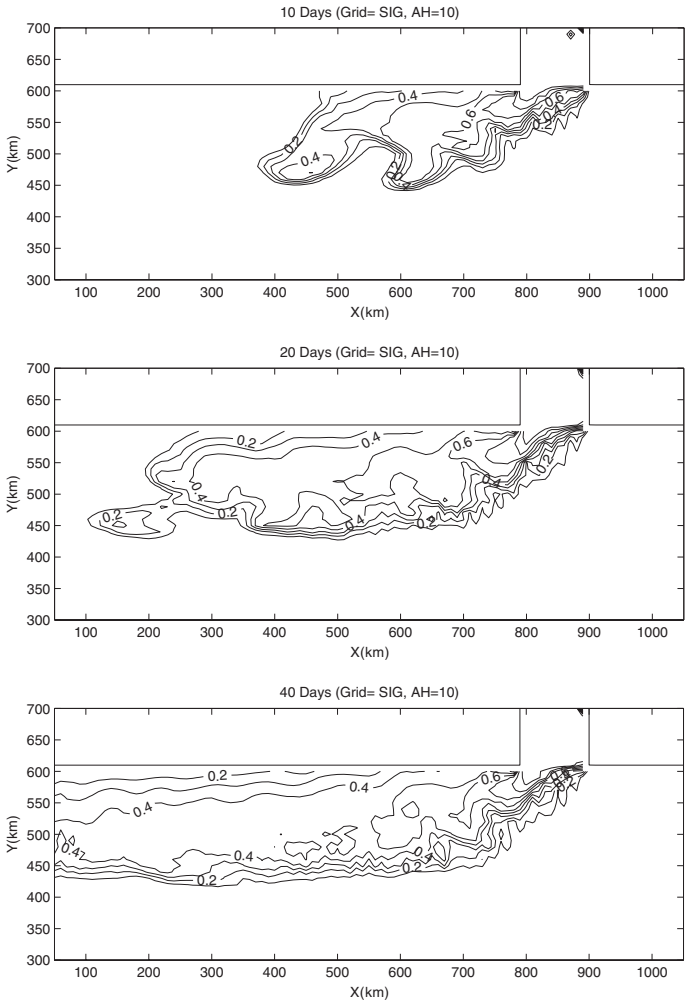


Fig. 5. Tracer concentration at the bottom layer after 10, 20 and 40 days simulation with the sigma grid (experiment S1, diffusivity $A_H = 10^1$ m$^2$ s$^{-1}$). Contour interval is 0.1.

calculations (Table 1). The plume thickness in the sigma models is quite close to the observed plume downstream of the Denmark Strait (Girton and Sanford, in press). It does seem that increasing the horizontal diffusivity in the $z$-level model results in increasing vertical mixing as well, this effect will be further discussed later.

To estimate the distribution of the water mass that originated from the dense water inflow source, we calculate the zonally averaged vertically integrated tracer concentration,

$$C(y,t) = \sum_x \sum_z c(x,y,z,t)\,\Delta x\,\Delta z \Big/ \sum_x .\Delta x; \tag{1}$$

this property for the different experiments is shown in Fig. 10 for $t = 40$ days. $C$ has units of meter and is proportional to the average thickness of the plume in the water column. In the sigma grid

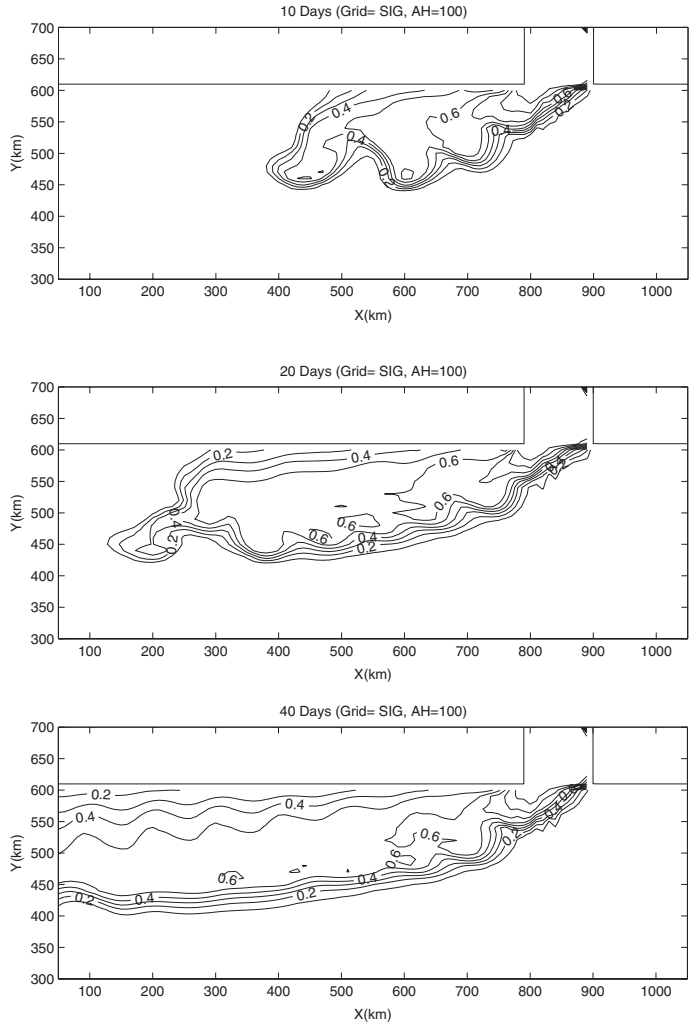


Fig. 6. Same as Fig. 5, but for experiment S2 ($A_H = 10^2$ m$^2$ s$^{-1}$).

calculations large portion of dense waters are found large distance from the coast (Fig. 10a), but in the $z$-level calculations the maximum thickness of the dense plume remains about 50 km from the coast with a sharp decline in the amount of dense water that reached farther downslope. The cases with the largest diffusivities, S3 and Z3, produce the largest amount of source water that reached farther offshore, however, in S3 these waters are near the bottom, while in Z3 they are mostly in the interior (Fig. 9); this result may explain the thick intermediate water mass found in the coarse resolution calculations (Fig. 3b).

To further investigate the dynamics of the BBL, Fig. 11 shows vertical profiles inside the plume (40 km downslope and 100 km downstream of the source, where the bottom depth is 1100 m). The profiles show much smaller downslope advection and larger vertical mixing in the $z$-level calculations than in the sigma grid calculations (Fig. 11c and d), which results in thicker and more

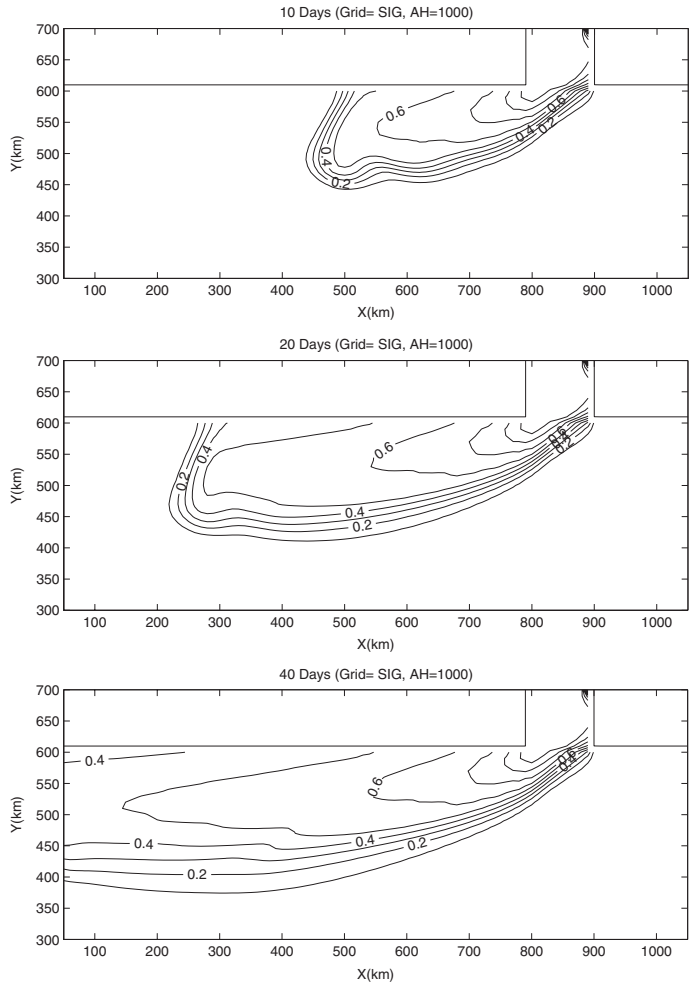


Fig. 7. Same as Fig. 5, but for experiment S3 ($A_H = 10^3$ m$^2$ s$^{-1}$).

diffused boundary layers in the $z$-grid (Fig. 11a and b). It is interesting to note that estimates of the average bottom mixed layer thickness of the Denmark Strait bottom plume, about 50–80 m (Girton and Sanford, in press), are very similar to the sigma model results of Fig. 11a, while the mixed layer thickness in the $z$-level model, about 250 m, seems too large. In the sigma grid, downslope Ekman veering and advection (and to lesser extent along-sigma diffusion. i.e., Fig. 9) produce a thin and stable BBL. In the $z$-level grid however, the downslope propagation of the plume involves two steps. First, the horizontal advection and diffusion mix the plume with water of adjacent grid cells which overlay grid cells below with less dense water; then, responding to the unstable stratification, the turbulence scheme creates large vertical mixing (see the schematic diagram of Fig. 12). A similar explanation has been offered by Winton et al. (1998), when comparing $z$-level and isopycnal models.

To compare the dynamical balances in the different grids we now look at the vertically integrated vorticity balance equation,

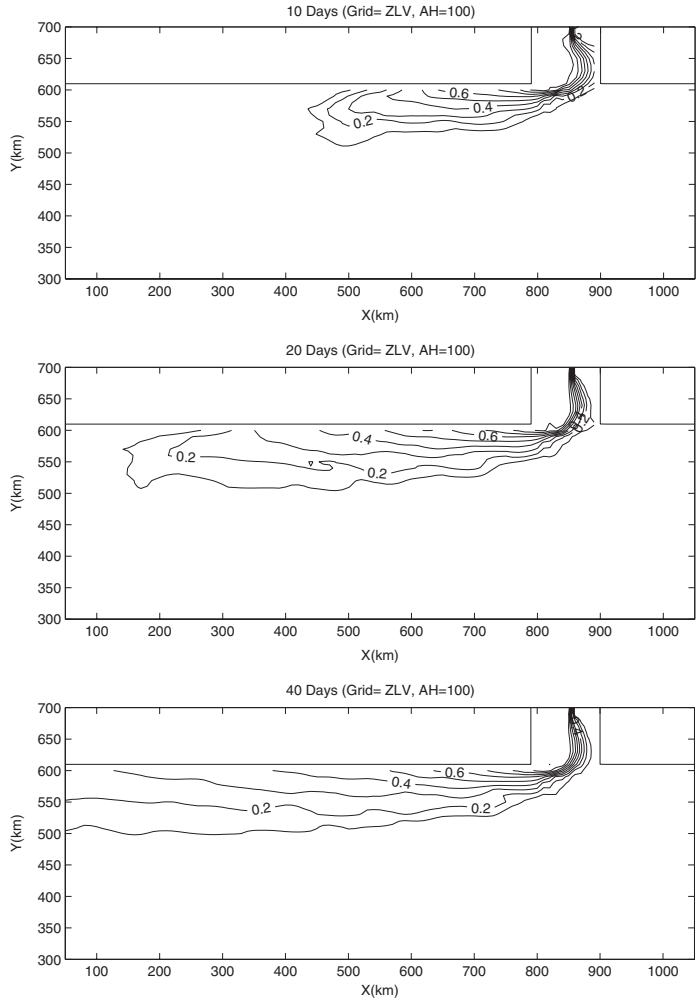


Fig. 8. Same as Fig. 5, but for the $z$-level model of experiment Z2 ($A_H = 10^2$ m$^2$ s$^{-1}$).

$$\frac{\partial}{\partial t}\left(\frac{\partial VD}{\partial x}-\frac{\partial UD}{\partial y}\right)+\left(\frac{\partial A_y}{\partial x}-\frac{\partial A_x}{\partial y}\right)+\left(\frac{\partial(fUD)}{\partial x}+\frac{\partial(fVD)}{\partial y}\right)+\left(-\frac{\partial P_b}{\partial x}\frac{\partial D}{\partial y}+\frac{\partial P_b}{\partial y}\frac{\partial D}{\partial x}\right)+\left(-\frac{\partial \tau_{yb}}{\partial x}+\frac{\partial \tau_{xb}}{\partial y}\right)=0, \tag{2}$$

where $(U, V)$ are the vertically averaged velocity components, $D = H + \eta$, $(A_x, A_y)$ are the advection and diffusion terms, $f$ is the Coriolis parameter, $P_b$ is the bottom pressure, and $(\tau_x, \tau_y)$ are the bottom stress components (surface stress is neglected in our case). The five terms in (2), the tendency term, the advection and diffusion term, the Coriolis term, the bottom pressure torque term, and the bottom stress term are calculated from the model results and shown in Fig. 13 for a section location as in Fig. 9. The general vorticity balance is quite similar for both grids, with the tendency term balanced by bottom pressure torque and advection terms; bottom stress and

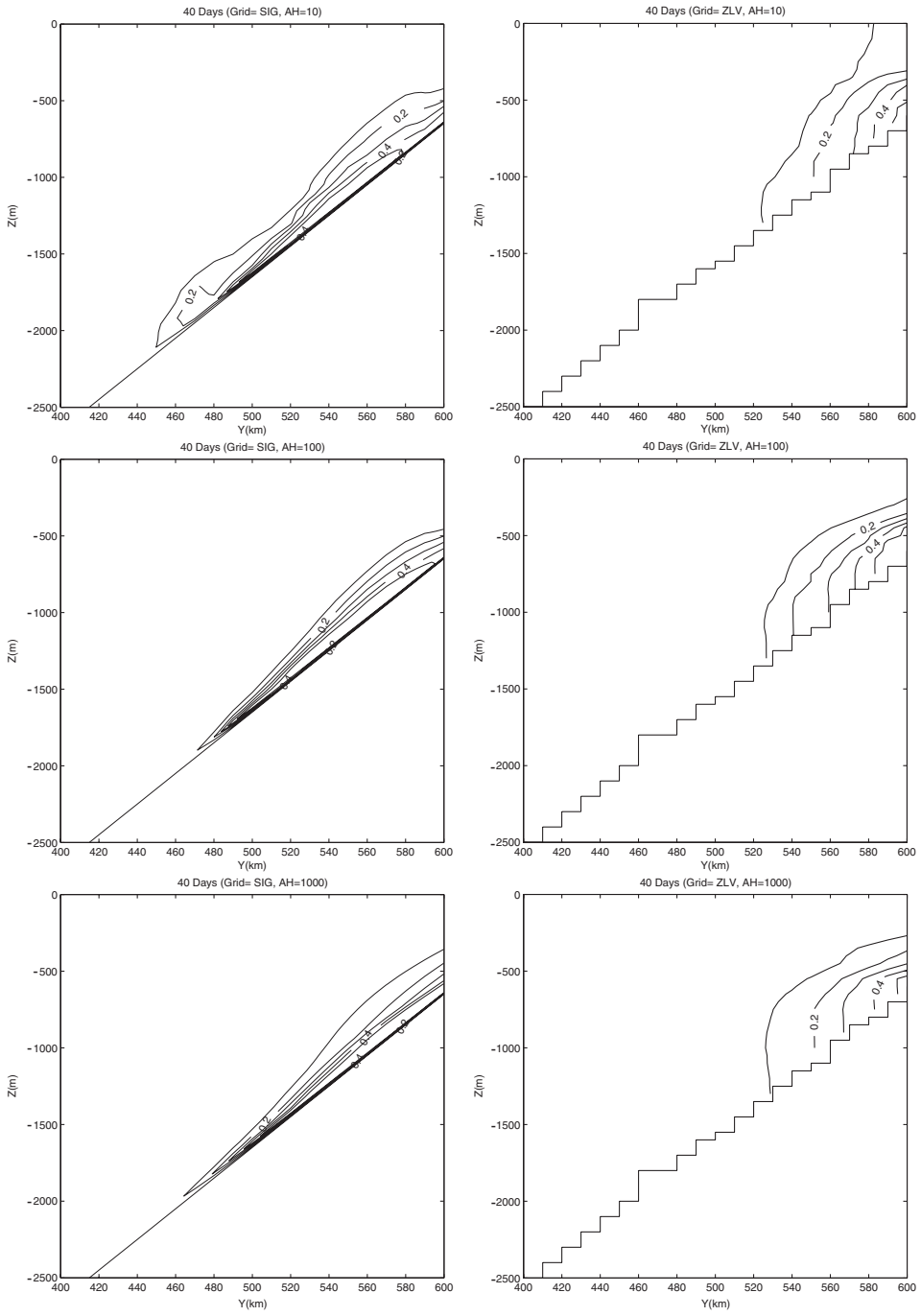


Fig. 9. Cross-section of tracer concentration 100 km downstream of the source, at $x = 700$ km, after 40 days simulation. Left panels are for the sigma coordinate experiments S1, S2 and S3, right panels are for the $z$-level experiments Z1, Z2 and Z3. Horizontal diffusivity increases from top to bottom. Contour interval is 0.1.

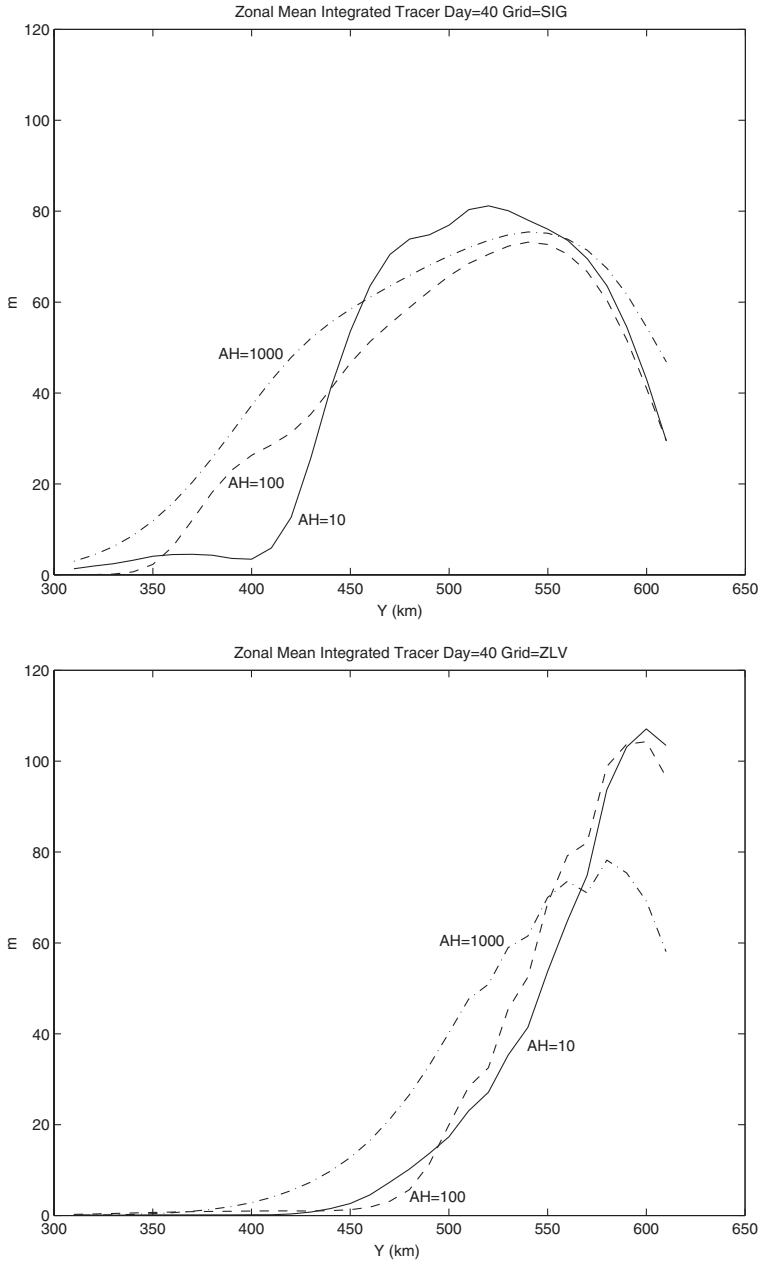


Fig. 10. Relative plume thickness (in meters) calculated by zonal and vertical integration of tracer concentration (see Eq. (1)) after 40 days simulations. The top panel is for the sigma grid calculations, and the bottom panel is for the $z$-level calculations. Solid, dash, and dash-dot lines represent cases with horizontal diffusivity of $10^1$, $10^2$, and $10^3$ $m^2\,s^{-1}$, respectively.

Coriolis terms play a lesser role (at least in the vertically integrated sense, though they are important very close to the bottom). However, in the $z$-level model the magnitude of the dominant

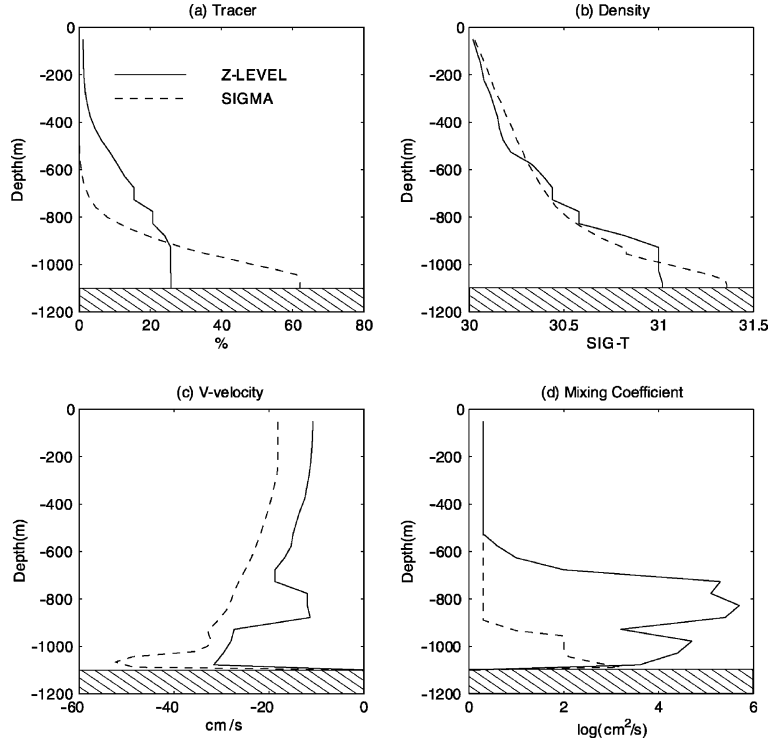


Fig. 11. Example of vertical profiles after 40 days at $(X, Y) = (700, 560$ km). (a) Tracer concentration (% of maximum concentration of the source), (b) density (in sigma-$t$ units), (c) across slope velocity (v-component, in cm s$^{-1}$), and (d) mixing coefficient (log of $K_M$ in cm$^2$ s$^{-1}$). Solid and dashed lines represent experiments Z2 and S2, respectively.

terms is about half of their magnitude in the sigma grid; this result is consistent with the more diffused plume and smaller bottom velocity in the $z$-level model as seen in Fig. 11. The momentum equation terms in the $z$-level grid are also spatially noisy due to the step-like discontinuity of the bottom topography, compared with smoother terms in the sigma grid. Fig. 14 shows the time-dependent nature of the absolute value of the vorticity terms, averaged over 200 km × 200 km box downstream of the embayment. While the $z$-level calculations reached some steady balance after 10–20 days, the terms in the sigma model calculations have not reached such a balance even after 40 days; the large tendency term indicate that westward propagating eddies dominate the vertically integrated vorticity. Nevertheless, a comparison of Fig. 13 with other sections in different locations or different times (not shown) indicate that the basic balance of terms remains the same, though the amplitude and sign may change with each passing eddy.

### 3.3. The effect of model grid resolution

Although the horizontal resolution and the number of vertical layers in experiments S1–S3 and Z1–Z3 are the same (so that the computational cost is similar as well), the actual vertical grid resolution is different, since the sigma grid by its nature has higher resolution in shallow regions and coarser resolution in the deep ocean (Table 1). For example, at the center of the plume,

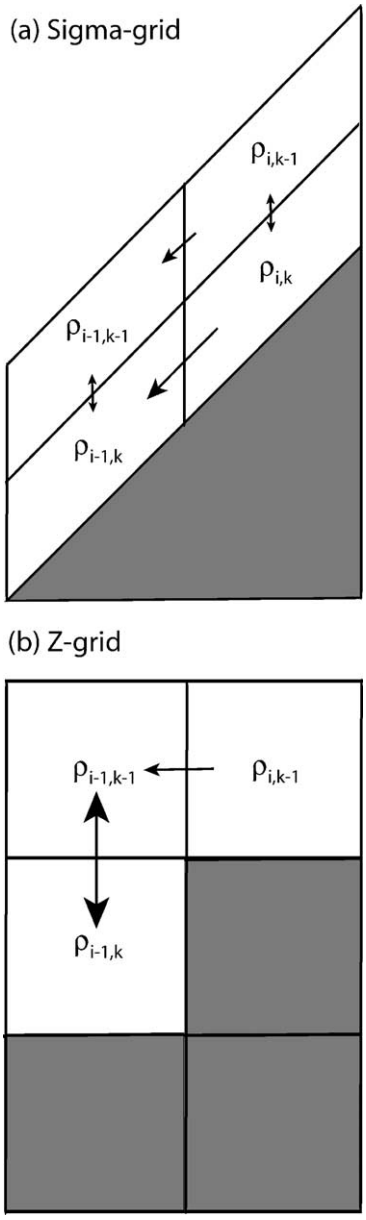


Fig. 12. Schematic diagram of the near bottom mixing processes near the edge of a dense plume for (a) sigma coordinate grid and for (b) $z$-level grid. Along-sigma advection is large in the sigma grid so that the densities $\rho_{i,k} \approx \rho_{i-1,k} > \rho_{i-1,k-1}$, while vertical mixing is large in the $z$-level grid so that $\rho_{i,k-1} > \rho_{i-1,k-1} \approx \rho_{i-1,k}$.

around 1000 m depth, the vertical resolution is about 20 m in the sigma grid and 50 m in the $z$-level grid. Therefore, the differences in the plume structure (Fig. 9) might be attributed to the higher vertical resolution (thus thinner BBL) in the sigma grid calculations. An additional experiment, S4, is thus performed with only 10 sigma layers, so that the vertical resolution at the

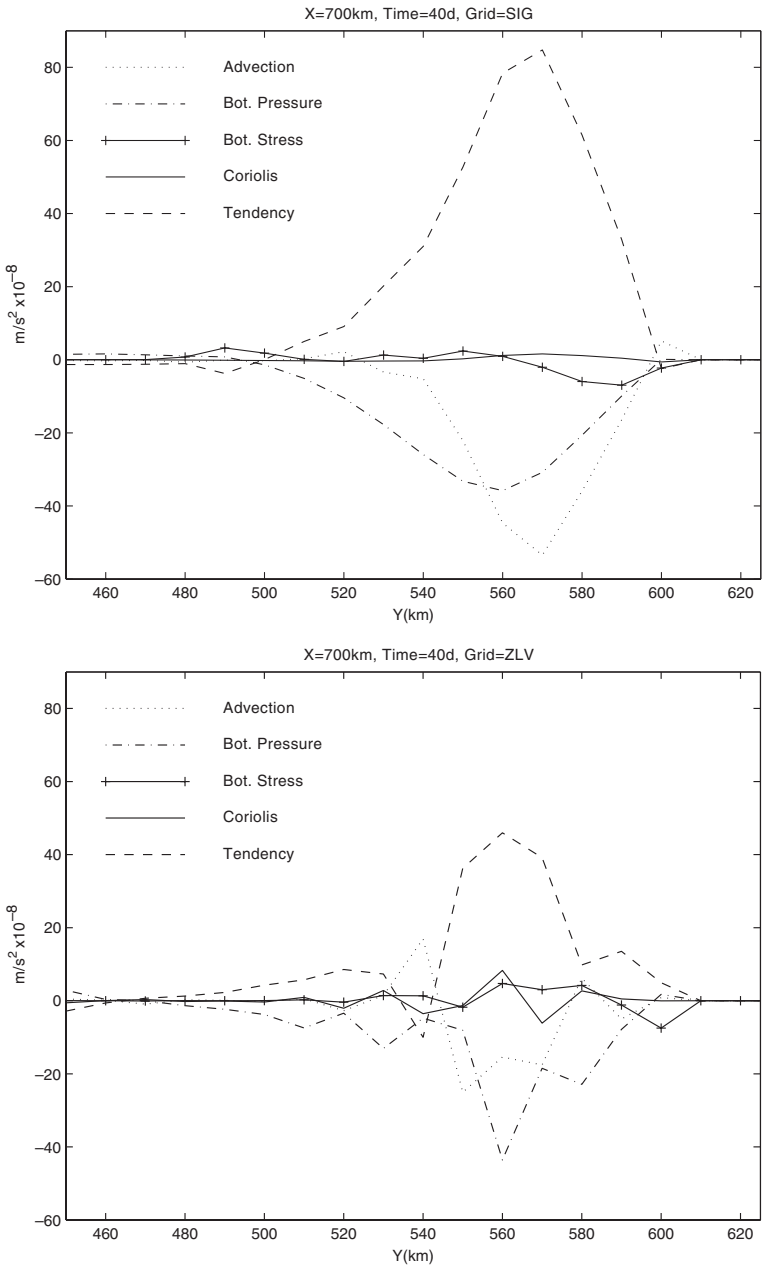


Fig. 13. The vertically integrated vorticity balance (see Eq. (2)) across $X = 700$ km after 40 days. Top panel is for experiments S2, bottom panel is for experiment Z2. The terms are the tendency (dashed line), advection and diffusion (dotted line), bottom pressure torque (dash-dot line), bottom stress ("+" line) and Coriolis (solid line).

shallowest region is 60 m, similar to the 50 m vertical resolution of the 50-layer $z$-level calculations. The results of this experiment after 40 days are shown in Fig. 15. Despite the lower resolution, the plume distribution along the slope is quite similar to the case with five times more

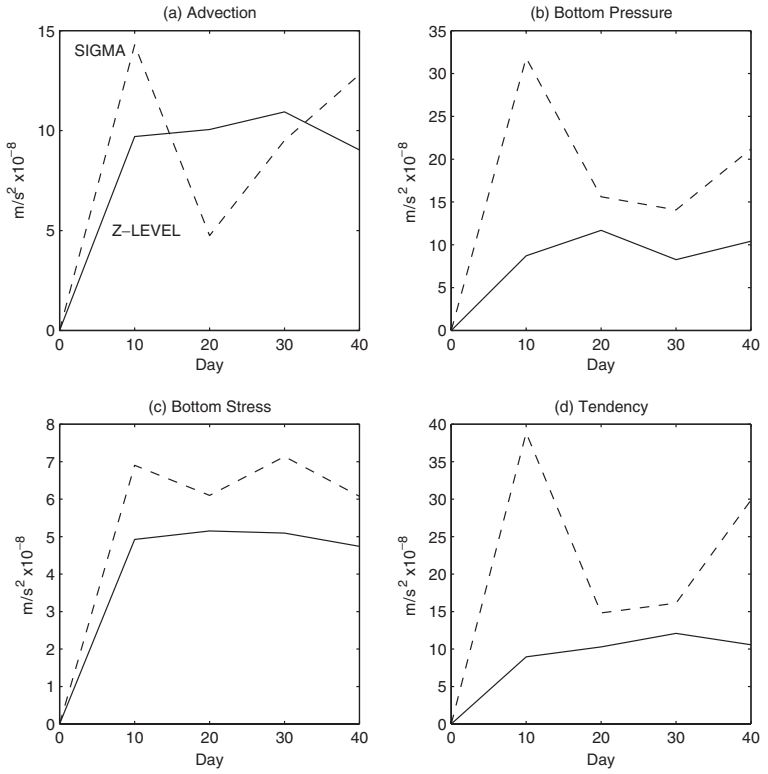


Fig. 14. The time-dependent nature of the magnitude of the dominant terms of the vorticity balance equation: (a) advection, (b) bottom pressure, (c) bottom stress, and (d) tendency. The units are the area average of the absolute values in the region 600 km $< X <$ 800 km and 400 km $< Y <$ 600 km. Solid lines represent the $z$-level model of experiment Z2 and dashed lines represent the sigma model of experiment S2.

vertical layers (Fig. 6). The average thickness of the plume has slightly increased (from 244 to 276 m, Table 1) and the mixed layer thickness more closely resembles that obtained in the $z$-level calculations (Fig. 9). In the coarse vertical resolution case, the downslope expansion of the dense water is somewhat decreased (the area of the plume is reduced by about 20% relative to S2, Table 1), but not as much as in the $z$-level cases (the plume area in Z2 is smaller than that in S2 by 45%, Table 1). Therefore we conclude that vertical resolution by itself is important to resolve the BBL, but is not the main cause of the limited plume expansion in $z$-level calculations.

Unlike sigma coordinates, increasing the vertical resolution alone in $z$-level coordinates may not result in a better resolved BBL because the vertical step height needs to be smaller than the BBL thickness. For example, the vertical scale of the thin BBL in the sigma calculations (left panels of Fig. 9) is of the same order as the steps in the 50-layers $z$-level calculations (right panels of Fig. 9). Therefore, both, horizontal and vertical resolutions must be increased, to achieve a better resolution of sloped topography in a $z$-level model. Thus, an additional $z$-level experiment is constructed, experiment Z4 (see Table 1), with much higher resolution, such that the bottom steps are smaller than the expected BBL thickness. In this experiment the horizontal resolution is quadrupled from 10 to 2.5 km grid and the vertical resolution is constant at 25 m. Because of the

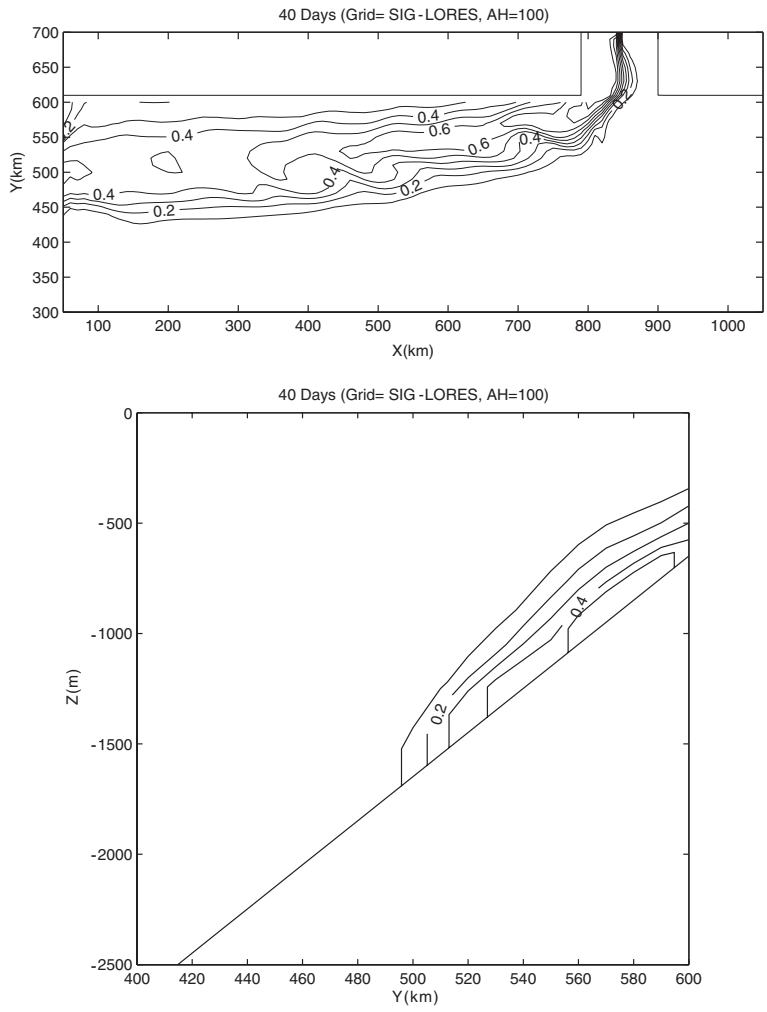


Fig. 15. Bottom tracer concentration (top panel) and cross section at $X = 700$ km (bottom panel) after 40 days simulation with a coarse vertical resolution sigma grid (experiment S4). Contour interval is 0.1.

enormous increase in computations for this case, a smaller domain is used (1100 km × 400 km, instead of 1100 km × 800 km), and the maximum depth is also reduced (2200 m instead of 3600 m) to allow a longer time step. The shortening of the domain in the $y$ direction only removes the region far away from the plume and thus should not affect the results. The plume structure in this very high-resolution case after 40 days is shown in Fig. 16, and should be compared with the bottom panel of Fig. 8 and the top panels of Fig. 9. The downslope extension of the plume is doubled now from about 50 km offshore to about 100 km (the total area of the plume increased by about 40%, Table 1), and the thickness of the BBL is smaller and more comparable with the sigma calculations (the average plume thickness in Z4, 272 m is almost identical to that in S4, 276 m, Table 1). During the development of the plume there are now more eddies (not shown) as obtained with the low diffusivity 10 km sigma grid (e.g., Figs. 5 and 6); such eddies were absent from

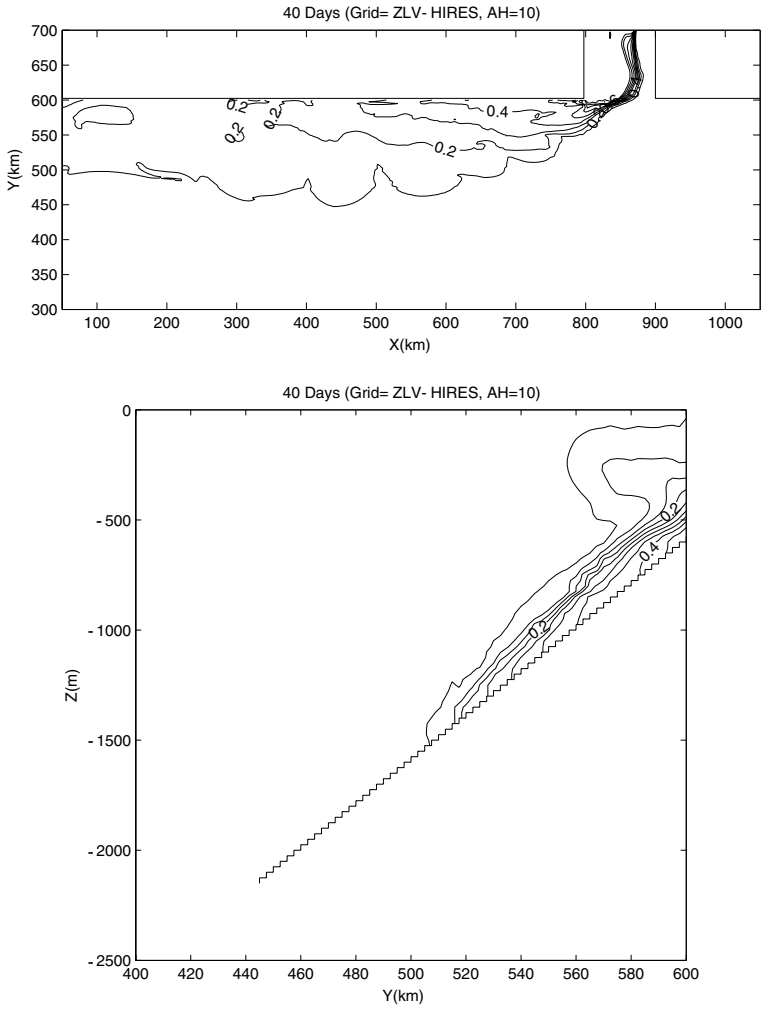


Fig. 16. Same as Fig. 15, but for simulation with very high-resolution (2.5 km) $z$-level grid (experiment Z4).

the 10 km $z$-level calculations because of the too diffused plume front. Despite the apparent convergent of the high-resolution $z$-level calculations to the solution obtained with the sigma grid, there are still some differences, and the amount of dense water further downstream is still smaller in the $z$-level than it is in the sigma grids. Even with a smaller grid, the basic differences in the BBL dynamics in different grids as depicted in Figs. 11 and 12 still exist, but are reduced. Large values of vertical mixing coefficients are still found in experiment Z4, but they are more confined to the few grid cells near the bottom.

## 4. Discussion and conclusions

With recent developments of various hybrid or general coordinate ocean models (Bleck, 2002; Mellor et al., 2002; Pietrzak et al., 2002; Rowley et al., 2002), users may have more flexibility in

the choice of the optimal model grid for a particular application. However, more research is needed to understand the effect of the model grid on the simulated results and how different choices of sub-grid scale parameterizations may relate to the grid used. Models with generalized grids give us the opportunity to isolate the effect of model grid on oceanic simulations while leaving other numerical aspects unchanged. The most apparent examples of cases where model results are strongly affected by the model grid are simulations of density-driven, down-slope flows since the grid determines how topography is represented in the model. The difficulty that $z$-level climate models have in simulating deep water formation processes is well documented (Gerdes, 1993; Adcroft et al., 1997; Beckmann and Döscher, 1997; Winton et al., 1998; Pacanowski and Gnanadesikan, 1998; Campin and Goosse, 1999; Killworth and Edwards, 1999; Song and Chao, 2000), and this motivated intercomparison projects such as the Dynamics of Overflow Mixing and Entrainment (DOME), and the recent Pilot Climate Process and Modeling Teams (CPT) initiative.

In this study the generalized coordinate ocean model of Mellor et al. (2002), applied to a large-scale climate simulation of deep water formation by high-latitude cooling, confirms previous studies with $z$-level models that indicate the need to add BBL schemes to $z$-level models; otherwise the step-like topography does not allow sufficient penetration of cold shelf water into the deep ocean. The experiments also show that, even with an idealized domain and a simple zonal forcing, terrain-following ocean models provide reasonable climatology and water masses. This may be important, since applications of terrain-following ocean models are being expanded now from their traditional coastal milieu to basin-scale climate milieu (Haidvogel et al., 2000; Hakkinen, 2000; Ezer and Mellor, 1997, 2000; Ezer, 1999, 2001).

High-resolution experiments evaluate the effect of various parameters on the evolution of a dense plume in sigma and in $z$-level models. The process of downslope spreading of a dense plume and its associated BBL dynamics depends strongly on the type of grid used and its resolution. In sigma coordinates (or other terrain-following coordinates) the process is dominated by downslope along-sigma advection driven by pressure gradients, with a thin (depending on sufficient vertical resolution) and stably stratified BBL. In $z$-level models, on the other hand, the BBL dynamics is a combination of horizontal advection and diffusion that creates hydrostatically unstable columns over the stepped topography that results in intense vertical mixing and thicker boundary layers. The size of the steps which depends on horizontal and vertical resolution determines, to a large extent, the thickness of the BBL. Because of this different BBL behavior, the sigma or $z$-level models respond differently to the choice of parameters and grid size, and this has been demonstrated here with various sensitivity experiments. For example, large horizontal diffusion (along the grid) increases the downslope extension and decreases the thickness of the plume in a sigma grid, but in $z$-level models it creates stronger vertical mixing, a thicker and more diffused plume that is limited in its downslope extension. Maintaining the plume's sharp front, results in frontal instability that causes meandering and eddies that further contribute to the mixing process (Jiang and Garwood, 1996). Eddies where obtained in the sigma grid calculations at 10 km resolution (and low-horizontal diffusivity), but in the $z$-level calculations they develop only at 2.5 km resolution. Increasing horizontal and vertical resolution in the $z$-level grid converges the results toward those obtained by a much coarser resolution sigma coordinate grid, but some differences remain due to the basic differences in the mixing process.

Despite the highly idealized model configuration, it is interesting to note that some of the basic features of the simulated overflow plume (e.g., in the sigma coordinate experiment S2) agree quite well with recent observations of the Denmark Strait plume (Girton and Sanford, in press). For example, the maximum velocity in the overflow layer is about 1.5 $m\,s^{-1}$ in the model, and about 1.3 $m\,s^{-1}$ in the observations, the average plume thickness is about 240 m in the model and 160 m in the observations, the mixed layer thickness is 50–100 m in the model and 50–80 m in the observations, and 100 km downstream from the source, the center of the plume descents from 600 m to about 1200 m depth in the model, and from 500 m to about 900 m in the observations. These encouraging results point to the need for more detailed model-data comparisons with more realistic model configurations; such experiments are planned in future studies.

Better understanding of the behavior of bottom mixing in ocean models using comparison studies of this type (either sigma-*z*-level comparisons as done here, or isopycnal-*z*-level comparisons as done by Winton et al., 1998, or model-data comparisons) may help in the ongoing developments of various BBL schemes for climate *z*-level models. Using subgrid-scale parameterizations that involve isopycnal instead of horizontal diffusion (Gent and McWilliams, 1990) may also improve density-driven deep water formation. Ocean models with generalized coordinate systems may also give modelers more flexibility to resolve complicated ocean topographies.

## Acknowledgements

The reseach is supported by ONR's Ocean Modeling and Prediction Program, contract number N00014-00-1-0228 (TE). GM is supported by ONR and NOPP grants. DOME participants, and in particular the current coordinators of the project, R. Hallberg (GFDL) and T. Ozgokmen (RSMAS), are thanked for many valuable discussions. Computational support was provided by NOAA's Geophysical Fluid Dynamics Laboratory.

## References

Adcroft, A., Hill, C., Marshall, J., 1997. Representation of topography by shaved cells in a height coordinate ocean model. Monthly Weather Review 125, 2293–2315.

Arakawa, A., Lamb, V.R., 1977. Computational design of the basic dynamical processes of the UCLA general circulation model. In: Methods in Computational Physics, vol. 17. Academic Press, New York, pp. 174–265.

Beckmann, A., Döscher, R., 1997. A method for improved representation of dense water spreading over topography in geopotential-coordinate models. Journal of Physical Oceanography 27, 581–591.

Beckmann, A., Haidvogel, D., 1993. Numerical simulation of flow around a tall isolated seamount. Journal of Physical Oceanography 23, 1736–1753.

Bleck, R., 2002. An oceanic general circulation model framed in hybrid isopycnic-cartesian coordinates. Ocean Modeling 4, 55–88.

Blumberg, A.F., Mellor, G.L., 1987. A description of a three-dimensional coastal ocean circulation model. In: Heaps, N.S. (Ed.), Three-Dimensional Coastal Ocean Models, Coastal Estuarine Studies 4. American Geophysical Union, Washington, pp. 1–16.

Campin, J.-M., Goosse, H., 1999. Parameterization of density-driven downsloping flow for a coarse-resolution ocean model in *z*-coordinate. Tellus 51A, 412–430.

Chassignet, E.P., Arango, H., Dietrich, D., Ezer, T., Ghil, M., Haidvogel, D.B., Ma, C.-C., Mehra, A., Paiva, A.F., Sirkes, Z., 2000. DAMEE-NAB: the base experiments. Dynamics of Atmospheres and Oceans 32, 155–183.

Chu, P.C., Fan, C., 1997. Sixth-order difference scheme for sigma coordinate ocean models. Journal of Physical Oceanography 27, 2064–2071.

Ezer, T., Arango, H., Shchepetkin, A.F., 2002. Developments in terrain-following ocean models. Intercomparisons of numerical aspects. Ocean Modelling 4, 249–267.

Ezer, T., 1999. Decadal variabilities of the upper layers of the subtropical North Atlantic: An ocean model study. Journal of Physical Oceanography 29, 3111–3124.

Ezer, T., 2000. On the seasonal mixed-layer simulated by a basin-scale ocean model and the Mellor–Yamada turbulence scheme. Journal of Geophysical Research 105, 16843–16855.

Ezer, T., 2001. On the response of the Atlantic Ocean to climatic changes in high latitudes: A sensitivity study with a sigma coordinate ocean model. In: Seidov, D., Maslin, M., Haupt, B. (Eds.), Ocean and Rapid Past and Future Climate Change: North-South connections, Geophysical Monograph, vol. 126, pp. 199–215.

Ezer, T., Mellor, G.L., 1997. Simulations of the Atlantic Ocean with a free surface sigma coordinate ocean model. Journal of Geophysical Research 102, 15647–15657.

Ezer, T., Mellor, G.L., 2000. Sensitivity studies with the North Atlantic sigma coordinate Princeton Ocean Model. Dynamics of Atmospheres and Oceans 32, 155–208.

Gent, P.R., McWilliams, J.C., 1990. Isopycnal mixing in ocean circulation models. Journal of Physical Oceanography 20, 150–155.

Gerdes, R., 1993. A primitive equation ocean circulation model using a general vertical coordinate transformation. 1. Description and testing of the model. Journal of Geophysical Research 98, 14683–14701.

Girton, J.B., Sanford, T.B., in press. Descent and modification of the overflow plume in the Denmark Strait. Journal of Physical Oceanography.

Griffies, S.M., Boning, C., Bryan, F.O., Chassignet, E.P., Gerdes, R., Hasumi, H., Hirst, A., Treguier, A., Webb, D., 2000. Developments in ocean climate modelling. Ocean Modelling 2, 123–192.

Haidvogel, D.B., Arango, H., Hedstrom, K., Beckmann, A., Malanotte-Rizzoli, P., Shchepetkin, A.F., 2000. Model evaluation experiments in the North Atlantic Basin: Simulations in nonlinear terrain-following coordinates. Dynamics of Atmospheres and Oceans 32, 239–282.

Hakkinen, S., 2000. Decadal air–sea interaction in the North Atlantic based on observations and modeling results. Journal of Climate 13, 1195–1219.

Haney, R.L., 1991. On the pressure gradient force over steep topography in sigma coordinate ocean models. Journal of Physical Oceanography 21, 610–619.

Jiang, L., Garwood Jr., R.W., 1996. Three-dimensional simulations of overflows on continental slopes. Journal of Physical Oceanography 26, 1214–1233.

Jungclaus, J.H., Hauser, J., Kase, R.H., 2001. Cyclogenesis in the Denmark Strait overflow plume. Journal of Physical Oceanography 31, 3214–3229.

Jungclaus, J.H., Mellor, G.L., 2000. A three-dimensional model study of the Mediterranean outflow. Journal of Marine Systems 24, 41–66.

Killworth, P.D., Edwards, N.R., 1999. A turbulent bottom boundary layer code for use in numerical models. Journal of Physical Oceanography 29, 1221–1238.

Levitus, S., Boyer, P., 1994. World Ocean Atlas 1994 Volume 4: Temperature. NOAA, NESDIS, Washington, DC, p. 117.

Meincke, J., Le Provst, C., Willebrand, J., 2001. Dynamics of the North Atlantic circulation (DYNAMO). Progress in Oceanography 48, 2–3.

Mellor, G.L., Blumberg, A.F., 1985. Modeling vertical and horizontal diffusivities with the sigma coordinate system. Monthly Weather Review 113, 1380–1383.

Mellor, G.L., Ezer, T., Oey, L.-Y., 1994. The pressure gradient conundrum of sigma coordinate ocean models. Journal of Atmospheric and Ocean Technology 11 (Part 2), 1126–1134.

Mellor, G.L., Hakkinen, S., Ezer, T., Patchen, R., 2002. A generalization of a sigma coordinate ocean model and an intercomparison of model vertical grids. In: Pinardi, N., Woods, J.D. (Eds.), Ocean Forecasting: Conceptual Basis and Applications. Springer, New York, pp. 55–72.

Mellor, G.L., Oey, L.-Y., Ezer, T., 1998. Sigma coordinate pressure gradient errors and the seamount problem. Journal of Atmospheric and Ocean Technology 15, 1122–1131.

Mellor, G.L., Wang, X.H., 1996. Pressure compensation and the bottom boundary layer. Journal of Physical Oceanography 26, 2214–2222.

Mellor, G.L., Yamada, T., 1982. Development of a turbulent closure model for geophysical fluid problems. Review of Geophysics 20, 851–875.

Pacanowski, R.C., Gnanadesikan, A., 1998. Transient response in a *z*-level ocean model that resolves topography with partial cells. Monthly Weather Review 126, 3248–3270.

Papadakis, M.P., Chassignet, E.P., Hallberg, R.W., 2003. Numerical simulations of the Mediterranean sea outflow: impact of the entrainment parameterization in an isopycnic coordinate ocean model. Ocean Modelling 5, 325–356.

Penduff, T., Barnier, B., Kerbiriou, M.-A., Verron, J., 2002. How topographic smoothing contributes to differences between the eddy flows simulated by sigma- and geopotential-coordinate models. Journal of Physical Oceanography 32, 122–137.

Pietrzak, J., Jakobson, J.B., Burchard, H., Vested, H.J., Peterson, O., 2002. A three-dimensional hydrostatic model for coastal and ocean modeling using a generalized topography following coordinate system. Ocean Modelling 4, 173–205.

Rochford, P.A., Kara, A.B., Wallcraft, A.J., Arnone, R.A., 2001. Importance of solar subsurface heating in ocean general circulation models. Journal of Geophysical Research 106 (C12), 30923–30938.

Rowley, C., Barron, C., Smedstad, L., Rhodes, R., 2002. Real-time ocean data assimilation and prediction with global NCOM. In: Oceans 2002. MTS/IEEE Publication, pp. 775–780.

Shchepetkin, A.F., McWilliams, J.C., 2003. A method for computing horizontal pressure gradient force in an ocean model with a non-aligned vertical coordinate. Journal of Geophysical Research 108 (C3), doi:10.1029/2001JC001-047.

Smagorinsky, J., 1963. General circulation experiments with the primitive equations: I. The basic experiments. Monthly Weather Review 91, 99–164.

Smolarkiewicz, P.K., 1984. A fully multidimensional positive definite advection transport algorithm with small implicit diffusion. Journal of Computational Physics 54, 325–362.

Song, Y.T., Chao, Y., 2000. An embedded bottom boundary layer formulation for *z*-coordinate ocean models. Journal of Atmospheric and Oceanic Technology 17, 546–560.

Song, Y.T., Haidvogel, D., 1994. A semi-implicit ocean circulation model using a generalized topography following coordinate system. Journal of Computational Physics 115, 228–248.

Willems, R.C., Glenn, S.M., Crowley, M.F., Malanotte-Rizzoli, P., Young, R.E., Ezer, T., Mellor, G.L., Arango, H., Robinson, A.R., Lai, C.-C., 1994. Experiment evaluates ocean models and data assimilation in the Gulf Stream. EOS Trans. Am. Geophys. Union 75 (34), 385–394.

Winton, M., Hallberg, R., Gnanadesikan, A., 1998. Simulation of density-driven frictional downslope flow in *z*-coordinate ocean models. Journal of Physical Oceanography 28, 2163–2174.

Zavatarelli, M., Mellor, G.L., 1995. A numerical study of the Mediterranean Sea circulation. Journal of Physical Oceanography 25 (6), 1384–1414.